analytical chemistry

pubs.acs.org/ac Article

Multiplexing of Electrospray Ionization Sources Using Orthogonal Injection into an Electrodynamic Ion Funnel

Pei Su,[§] Xi Chen,[§] Andrew J. Smith, Michael F. Espenship, Hugo Y. Samayoa Oviedo, Solita M. Wilson, Habib Gholipour-Ranjbar, Carlos Larriba-Andaluz, and Julia Laskin*

Cite This: https://doi.org/10.1021/acs.analchem.1c02092 Read Online

ACCESS | Metrics & More | Article Recommendations | Supporting Information

ABSTRACT: In this contribution, we report an efficient approach to multiplex electrospray ionization (ESI) sources for applications in analytical and preparative mass spectrometry. This is achieved using up to four orthogonal injection inlets implemented on the opposite sides of an electrodynamic ion funnel interface. We demonstrate that both the total ion current transmitted through the mass spectrometer and the signal-to-noise ratio increased by 3.8-fold using four inlets compared to one inlet. The performance of the new multiplexing approach was examined using different classes of analytes covering a broad range of mass and ionic charge. A deposition rate of >10 μg of mass-selected ions per day may be achieved by using the multiplexed sources coupled to preparative mass spectrometry. The almost proportional increase in the ion current with the number of ESI inlets observed experimentally is confirmed using gas flow and ion trajectory simulations. The simulations demonstrate a pronounced effect of gas dynamics on the ion trajectories in the ion funnel, indicating that the efficiency of multiplexing strongly depends on gas velocity field. The study presented herein opens up exciting opportunities for the development of bright ion sources, which will advance both analytical and preparative mass spectrometry applications.

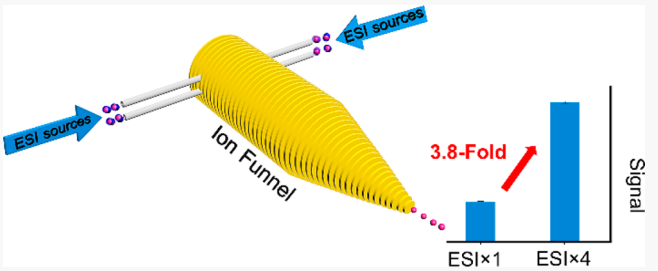

INTRODUCTION

Electrospray ionization (ESI) is a widely used atmospheric pressure ionization technique in mass spectrometry (MS).[1,2] In ESI, an electric field applied to the liquid meniscus formed at the tip of a capillary produces a Taylor cone, from which charged microdroplets are generated containing analyte molecules.[3] Subsequent desolvation of the microdroplets produces bare or partially solvated ions that are analyzed by a mass spectrometer.[4,5] Soft ionization with minimal fragmentation,[6] compatibility with liquid-phase separation techniques,[7,8] access to a wide range of molecular ions,[6,9,10] along with simplicity and ease of operation make ESI particularly attractive for both analytical and preparative MS applications.[11−14]

Since the initial demonstration of ESI-MS, the scientific community has been on the quest for improving the efficiency by maximizing the ion flux provided by this powerful ionization technique. The dramatic improvements in the sensitivity of ESI-MS achieved through these efforts have opened up a wide range of applications in biological research,[15] forensics,[16] environmental sciences,[17] drug discovery,[18] and clinical studies.[19,20] Moreover, preparative MS applications of interest to materials science,[21,22] energy production and storage,[23,24] catalysis,[25,26] and molecular electronics[27] have been transformed by the development of brighter ESI sources. Many studies have focused on the efficient transfer of ESI-generated ions into the vacuum system of a mass spectrometer.[28−30] The inner diameter and length of the heated inlet have been optimized, and specially shaped heated capillary inlets have been developed to increase ion transmission in the atmosphere−vacuum interface.[31−34] Alternatively, a sub-ambient-pressure ESI source interfaced with an electrodynamic ion funnel may be used to generate ions inside the vacuum system, thereby preventing ion loss in the capillary inlet.[35] Ambient-pressure ion funnel systems have also been developed to enhance the transmission of ions.[36,37]

Nonetheless, further improvement in the ion current from a single emitter is limited by the smallest droplet size that can be generated at a given flow rate and the maximum amount of charge carried by the ESI droplets, which is known as the Rayleigh limit.[38−40] Multiplexing of the ESI emitters is a promising strategy that has been employed to overcome this limitation.[41−45] One multiplexing strategy involves the development of ESI emitter arrays, which have been used both in analytical MS[46,47] and ESI-based propulsion.[48,49] In

Received: May 18, 2021
Accepted: August 2, 2021

analytical MS, a circular 22-emitter array has been used to achieve more than a 2-fold improvement in the MS sensitivity.[50] Ambient ion beam merging and focusing using specially shaped 3D-printed devices and counter-propagating beams provides an opportunity to manipulate and combine multiple ion beams before they enter the vacuum system.[51,52] Despite the significant progress in this field, multiplexing of ion beams still results in a substantial ion loss, which motivates the development of new multiplexing strategies.

An electrodynamic ion funnel is commonly used in both commercial and custom-designed mass spectrometers to facilitate ion transmission in the ESI interface.[53] An ion funnel is composed of a stack of ring electrodes operated using radio frequency and direct current voltages to efficiently focus and transmit ions at subambient pressures (0.5−30 Torr).[54] Ion funnels are commonly used in conjunction with ESI and heated capillary inlets. An ESI-generated ion beam is typically injected along the axis of the ion funnel. Orthogonal injection of ions from a heated inlet through a cutout section on one side of the ion funnel has also been demonstrated.[55] This configuration provided a 2−3-fold increase in ion transmission in comparison with axial injection.[34] Furthermore, a substantial improvement in the ion current was obtained by increasing the inner diameter of the heated inlet from 0.76 to 1.17 mm. However, further increase in the inner diameter of the heated inlet did not improve the observed mass-selected ion current. Another advantage of orthogonal injection is that it efficiently eliminates neutral contaminants and noninertial droplets entrained with the gas flow into the vacuum system, which has been shown to improve the analytical performance of a mass spectrometer.[55]

Herein, we present an approach for efficient multiplexing of independent ESI sources using multiple orthogonal injections into an ion funnel. We demonstrate that multiplexing of four orthogonal inlets results in an almost proportional increase in the total ion current and signal-to-noise ratio as compared to a single orthogonal inlet. In our approach, two pairs of heated inlets are mounted on the opposite sides of the ion funnel, and each inlet is equipped with an independently operated ESI emitter. Gas flow and ion trajectory simulations provide insights into factors affecting the efficient merging of ion beams using orthogonal injection of multiple ion beams into an ion funnel. The simulations demonstrate that the velocity and direction of the gas flows generated by the individual inlets are critical factors determining the ion extraction efficiency from the gas stream into the ion funnel. In addition, simulations at different gas pressures were used to identify the optimal pressure for merging four inlets of 1 mm inner diameter. The optimal pressure of ∼7 Torr obtained in simulations is in good agreement with the experimental data.

EXPERIMENTAL SECTION

Tris(2,2′-bipyridyl)dichlororuthenium(II) hexahydrate ($[Ru(bpy)_3]\cdot 6H_2O$, CAS: 50525−27−4), sodium phosphotungstate tribasic hydrate ($Na_3[PW_{12}O_{40}]\cdot xH_2O$, CAS: 12026−98−1), substance P acetate salt hydrate (CAS: 137348−11−9, anhydrous), and ubiquitin from bovine erythrocytes (≥98% purity, CAS: 79856−22−4) were purchased from Sigma-Aldrich (St. Louis, MO) and used as received. Tetrabutylammonium-chlorinated dodecaborate ($(TBA)_2B_{12}Cl_{12}$) salt was kindly provided by Drs. Jonas Warneke and Carsten Jenne. $Na[V_6O_7(OCH_3)_{12}]$ and $[Co_6S_8(PEt_3)_6]Cl$ were synthesized according to reported procedures.[56,57] Substance P was dissolved in a 9:1 (v/v) methanol/H_2O solution to a concentration of 100 μM. Ubiquitin ions were dissolved in $CH_3OH/H_2O/CH_3COOH$ = 49.5/49.5/1% solution to a concentration of 20 μM. Unless specified otherwise, other analytes were dissolved in methanol at a concentration of 150 μM.

The multiplexed electrospray ionization (ESI) interface is implemented on a custom-designed dual-polarity ion soft landing instrument described in detail elsewhere.[58] Briefly, the instrument is equipped with a high-transmission ESI interface (Spectroglyph, LLC) composed of a tandem electrodynamic ion funnel system and a bent flatapole ion guide (Figure S1).[58] A high-pressure ion funnel (HPF) is housed in a vacuum chamber differentially pumped to 7 Torr by a dry screw vacuum pump (VARODRY VD200, 118 cubic feet per minute (cfm), Leybold GmbH, Cologne, Germany). The pumping port is located downstream from the inlets close to the next vacuum chamber. Typical pressures in the chambers that house the low-pressure ion funnel (LPF) and the bent flatapole ion guide are 0.8 Torr and 10−20 mTorr, respectively. The fourth vacuum stage, in which ion current detection and ion beam characterization are performed, is differentially pumped to 3−6 × 10^{-5} Torr.

The high-transmission ESI interface described in our previous publication is equipped with two orthogonal injection ESI sources.[58] Ions are introduced into vacuum through stainless-steel heated inlet tubes from the opposite sides of the HPF. Each inlet tube is mounted on a stainless-steel cartridge (Figure 1a, top left corner). The temperature of each heated inlet is maintained by a cartridge heater and a thermocouple. A detailed drawing of the cartridge is shown in Figure 1a. In particular, two inlets (1/16″ OD, 0.04″ ID, 7 cm length, VICI Valco Instruments, Houston, TX) are inserted through two channels drilled through the cartridge that are spaced by 6 mm. We selected 0.04″ ID inlets for multiplexing. This ID is close to the optimum value reported in our previous study[34] and was selected by considering the available pumping power. Two 2[illegible] V, 60W cartridge heaters (1/8″ dia., 1−1/4″ long, Gordo[illegible] Sales, Layton, UT) are connected in series and inserted into the side channels of the cartridge to provide sufficient heating power for efficient desolvation of the ESI droplets. A thermocouple wire is inserted into another channel between the heaters. The temperature of the cartridges is maintained at 180 °C.

The HPF shown in Figure 1a,b and described in our previous publication[58] is composed of a repeller section and a funnel-shaped section. The heated inlets are inserted into the HPF through two cutouts (10 × 10 mm) on the opposite sides of the repeller section. Introducing the ion beams through the funnel section, which was not explored in this work, may require a different radio frequency (RF) potential well. The cutouts are staggered along the HPF axis and separated by 5 mm. The heated inlets protrude into the cutouts of the HPF by ∼1 mm, which is the optimized position for ion transmission. A front view of the ion funnel when the four orthogonal inlets are inserted into the funnel is shown on the right side of Figure 1b. Same direct current (DC) voltages are applied to the all the inlets.

Ions are generated using direct infusion ESI at a typical flow rate of 60 μL/h. Charged microdroplets are produced by applying a ±3 kV voltage to the stainless-steel syringe needle. The microdroplets are transferred into the ion funnel through a heated inlet, where desolvation takes place to generate ions.

https://doi.org/10.1021/acs.analchem.1c02092
Anal. Chem. XXXX, XXX, XXX−XXX

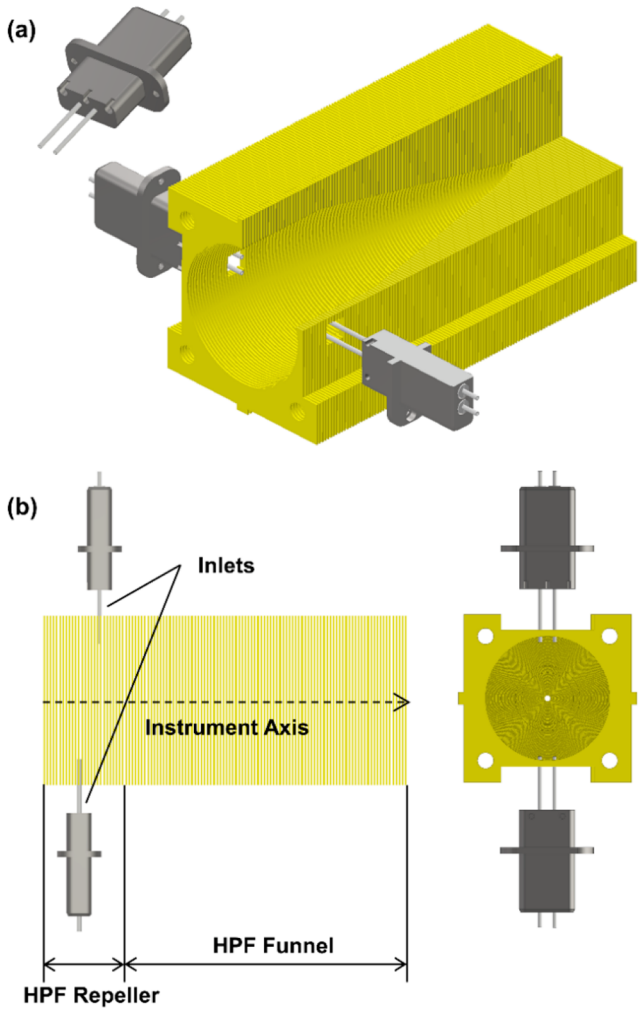

Figure 1. (a) Sectioned 3D drawing of the funnel with two two-inlet cartridges. A diagram of the two-inlet cartridge used for multiplexing experiments is shown on the top left corner. (b) Top (left) and front (right) view of the multiplexed ion funnel equipped with four heated inlets. The HPF repeller and funnel section are labeled in the schematic diagram on the left.

In the multiplexed mode where more than one ESI emitter is used to generate ions, each emitter is aligned with a specific heated inlet, and the same potential is applied to all the inlets. The ESI emitters that introduce ions from the same side of the HPF are mounted onto a 3D-printed bracket positioned in front of the heated inlets using a three-axis dovetail translation stage (DT12XYZ, Thorlabs Inc., Newton, NJ). Although the initial multiplexing experiments were performed using separate syringes interfaced with each ESI emitter, the complexity of the system may be reduced using T-unions for branching out the infusion lines from one syringe. In addition, quantity-limited samples for analytical applications may need to be diluted for injection into the multiplexed sources. However, this is not a concern for preparative mass spectrometry where sample is typically not quantity-limited.

In a typical experiment, an orthogonally injected ion beam is transferred through the HPF and LPF into the bent flatapole ion guide where collisional cooling takes place. Ions are subsequently transferred into a high-vacuum chamber and mass-selected using a quadrupole mass filter (Extrel CMS, Pittsburgh, PA), focused by an einzel lens, and directed onto a current collector plate connected to a picoammeter (RBD Instruments, Bend, OR) for ion current measurement. The picoammeter is typically operated at a sampling rate of 300 ms, and the current reported for a specific ion is averaged over a time period of >30 s.

The analytical performance of the multiplexed source is evaluated using a mass-dispersive rotating wall mass analyzer (RWMA) described in detail elsewhere and in the Supporting Information.[59,60] The transmitted ion current of a particular analyte is characterized by its peak intensity on an averaged ion beam profile obtained using a position sensitive IonCCD detector (OI Analytical, Pelham, AL). The signal intensity in the averaged IonCCD profile is obtained using a Lorentzian curve fitting, from which the peak height is extracted. The noise level is analyzed using a section of the IonCCD profile in the range of x = (−5, 5 mm) where no distinct ion signal is observed. The noise region of the IonCCD profile is first fitted with a third-order polynomial using a Savitzky-Golay filter with a 50-point window. The noise level is extracted by calculating the standard deviation of the experimental profile from the fitted profile. The SNR is obtained by taking the ratio of the peak height to noise level.

Gas flow simulations inside the multiplexed HPF were performed using the computational fluid dynamic (CFD) package in Solidworks (version 2017 SP0, Waltham, MA). Solidworks is a solid modeling computer-aided design (CAD) software, which utilizes a parametric feature-based approach to build up models and assemblies. Gas flow simulations utilized Flow Simulation, a module in Solidworks that numerically analyzes the flow inside the region considered to be the fluid domain. The ion funnel model was recreated with as much fidelity to the experimental version as possible. The model included the inlet tubes, stack of ring electrodes, and the HPF vacuum chamber with a pumping port. Solidworks employs finite volume methods to run flow simulations due to their ability to conserve flow properties (i.e., mass, momentum, and energy). Once the geometric model is constructed, Solidworks "meshes" the system by dividing the model into simple shapes, in this case hexahedral. Although the first meshing is coarse and performed automatically, it can be further refined. Refining is important in places where abrupt flow changes may occur so that the dynamics of the flow are accurately evaluated. As such, the mesh was refined close to the capillaries and the surfaces of the HPF. To predict turbulence, we used the Favre-averaged Navier−Stokes equations, which incorporate time-averaged effects of the turbulence perturbations. When these equations are employed, extra stresses (known as Reynolds stresses) appear in the equations, which are described using transport equations for the turbulent kinetic energy and its dissipation rate in what is known as the $k - \epsilon$ model. Solidworks has the option to use a different set of interconvertible variables known as turbulence intensity (Tu) and turbulence length scale (Tu_L). The typical values of Tu and Tu_L are 3% and 0.001 m, respectively. For the boundary conditions, the experimentally measured pressures at the entrance (atmospheric pressure) and exit (3−11 Torr) of the inlet tubes as wel as at the HPF exit (0.1−3 Torr) were applied. A temperature of 305 K was applied on the inlet tubes in the simulation and to the outside walls of the system. Once the simulation converged (around 300∼400 iterations) and a steady state was reached, the velocity data as a function of position was recorded.

Simulations of ion trajectories in the presence of the electric field and gas flow were performed using SIMION software

https://doi.org/10.1021/acs.analchem.1c02092
Anal. Chem. XXXX, XXX, XXX−XXX

package (version 8.1.1.32, Scientific Instrument Services, Ringoes, NJ). The electric field was generated through a combination of DC and RF voltages applied to the electrodes, mimicking the voltages from the experiment. SIMION allows the user to incorporate a velocity field to the ion simulations, which was obtained from the CFD simulations. Since the grid in the SIMION simulation is different from the grid employed in Solidworks, MATLAB was used to interpolate the results and transform the velocity field into a suitable grid. A program was written in SIMION using the Lua programming language to couple the effects of electric and flow fields. The hard sphere HS1 collision model in SIMION typically employed in low-pressure environments was used to simulate collisions of ions with background gas. In this model, the ions are considered to be spherical, and the ion−neutral interaction potential is represented by a step function. Simulations were performed using ions of m/z = 608 corresponding to triply charged $PMo_{12}O_{40}^{3-}$ species. To sample the ion trajectories, 40 ions (10 for each inlet) were initially positioned randomly at the end of the inlet tubes within a circle of 3 mm in diameter to account for diffusion. The number of ions involved in the simulation was selected based off the computational power available. Their initial velocity was equal to the inlet flow velocity (~400 m/s), and its direction was randomly selected from within a cone of a half angle of 15° pointing away from the inlet tube. The time-step size of 0.05 μs used in the simulations is a small fraction of the RF period, which was selected to properly account for the RF effects on ion trajectories. Decreasing the time-step beyond this value would greatly increase the computational time. Space charge was not considered in these initial simulations.

RESULTS AND DISCUSSION

In this study, we demonstrate that orthogonal injection into an ion funnel is an efficient approach to the multiplexing of electrospray ionization (ESI) sources. Specifically, we modified the dual-ion funnel interface in our laboratory to combine four ion beams in the high-pressure funnel (HPF, Figure 1). Because the cutouts in the HPF are offset relative to each other, we could only explore a "staggered" configuration of the multiplexed inlets experimentally. The number of inlets was selected based on the size of the cutouts in the HPF and the maximum pumping speed available in the lab. We use an ESI×n (n = 1−4) notation to represent the number of inlets used to introduce ion beams generated from individual ESI emitters in different instrument configurations examined in this study. Specifically, ESI×1 corresponds to one ESI emitter interfaced with one of the four inlets, ESI×2 corresponds to two emitters interfaced with two inlets, and so on. To evaluate the applicability of the multiplexing approach to different types of analytes, we selected several model systems representing different classes of compounds of interest to both analytical and preparative mass spectrometry (MS) applications.

We first characterized the analytical performance of the multiplexed interface by systematically introducing ion beams of a single-component solution through a different number of inlets while keeping the same gas flow into the HPF vacuum chamber. The ion beam was analyzed using a mass-dispersive device, rotating wall mass analyzer (RWMA), and an IonCCD detector. The RWMA separates ions onto spatially distinct rings based on their m/z. Each ring generates a pair of signals symmetrically located around the center of the one-dimensional IonCCD profile. The resulting spatial distribution of ions visualized using IonCCD is a mass spectrum composed of two distributions that are mirror images of one another.

Typical IonCCD profiles obtained at a frequency of 50 kHz for $Ru(bpy)_3^{2+}$ and substance P in ESI×n (n = 1−4) modes are shown in Figure 2a,b, respectively. In the profiles, the signal is

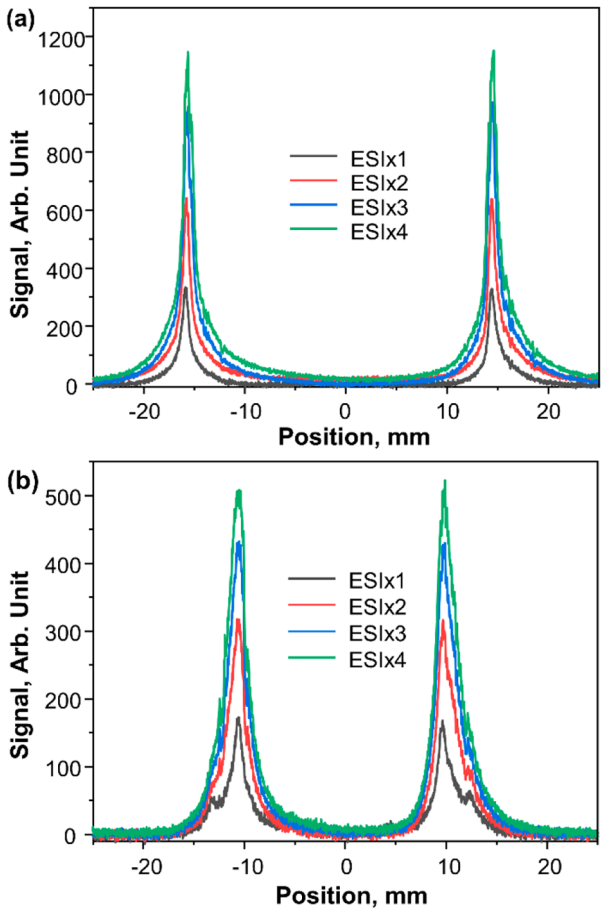

Figure 2. IonCCD profiles of $Ru(bpy)_3^{2+}$ (a) and substance P (b) in ESI×n (n = 1−4) modes.

plotted as a function of the position on the IonCCD, which is directly related to m/z. The pair of peaks in each profile in Figure 2a is assigned to $Ru(bpy)_3^{2+}$ at m/z 285. Meanwhile, IonCCD profiles obtained for substance P (Figure 2b) contain two pairs of peaks: the abundant signals at ±10 mm and lower-abundance signals at ±12 mm assigned to $[M + 2H]^{2+}$ and $[M + 3H]^{3+}$ ions,[61] respectively, using the calibration procedure described in detail in our previous study.[60] The $[M + 3H]^{3+}$ signal is clearly observed in the IonCCD profile obtained in the ESI×1 mode (black trace) but is lower in abundance and observed as a pair of shoulder peaks in IonCCD profiles obtained in the ESI×n (n = 2−4) modes.

For both model systems, we observe a gradual increase in signal with an increase in the number of ESI emitters from one (ESI×1 mode, black trace) to four (ESI×4 mode, green trace). The absolute signals and signal-to-noise ratios (SNRs) obtained for $Ru(bpy)_3^{2+}$ and substance P $[M + 2H]^{2+}$ are shown in Figure 3. We observe that the signal intensity increases almost proportionally to the number of inlets with a slightly smaller increase from the ESI×3 to ESI×4 modes. Meanwhile, the noise level in the IonCCD profiles is the same in all the ESI×n (n = 1−4) modes. The resulting SNR values

https://doi.org/10.1021/acs.analchem.1c02092
Anal. Chem. XXXX, XXX, XXX−XXX

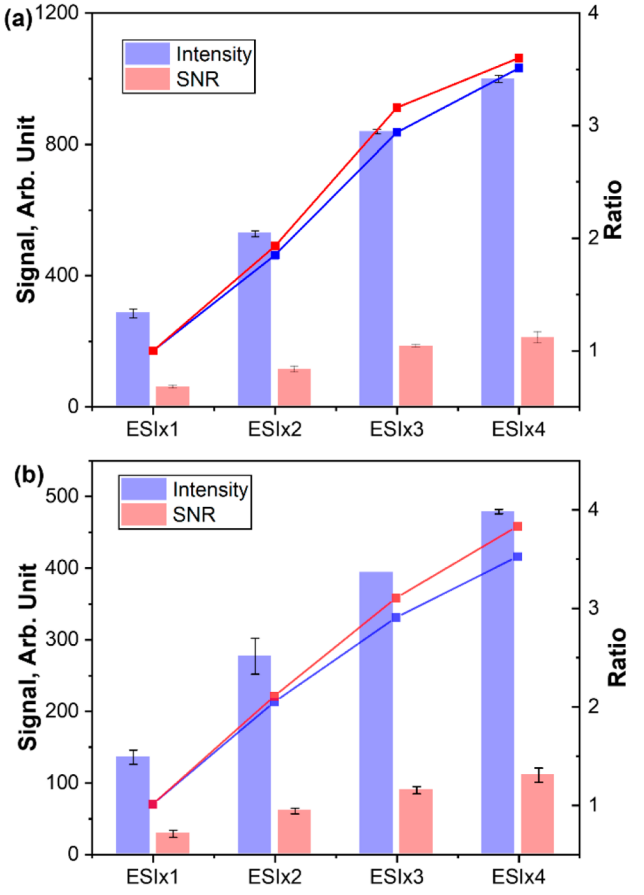

Figure 3. Peak intensities and SNRs extracted from the positive portion of the IonCCD profiles of $Ru(bpy)_3^{2+}$ (a) and substance P $[M + 2H]^{2+}$ (b) shown in Figure 2 using the Lorentzian curve fitting. The blue and red bars/plots correspond to intensity and SNR of the signal in each panel.

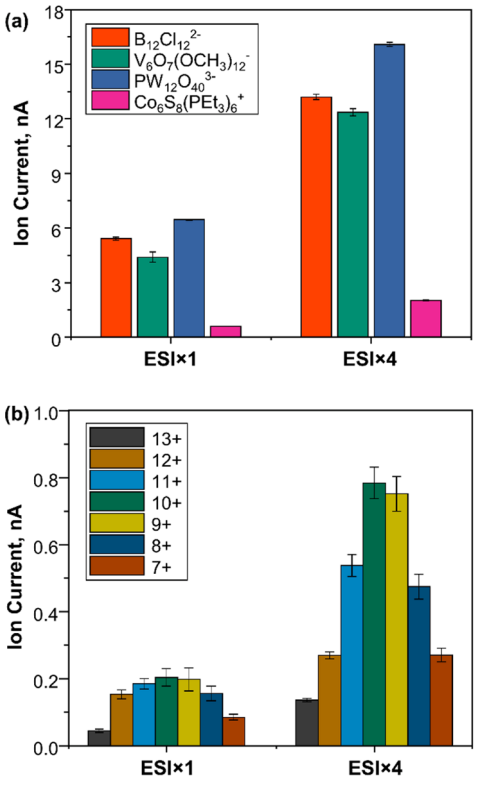

Figure 4. Mass-selected ion current obtained for (a) four model cluster ions, $B_{12}Cl_{12}^{2-}$, $V_6O_7(OCH_3)_{12}^-$, $PW_{12}O_{40}^{3-}$, $Co_6S_8(PEt_3)_6^+$, and (b) different charge states of ubiquitin (from 13+ to 7+) in the ESI×1 and ESI×4 modes.

follow the same trend as peak heights. This analysis indicates that multiplexing of four ESI sources results in a 3.6- and 3.8-fold increase in both the signal and SNR for $Ru(bpy)_3^{2+}$ and substance P $[M + 2H]^{2+}$, respectively.

However, for substance P, the trend is more linear, resulting in a 3.8-fold increase in both the signal and SNR between the ESI×1 and ESI×4 modes. The observed difference between $Ru(bpy)_3^{2+}$ and substance P data may be attributed to the higher overall ion current obtained for $Ru(bpy)_3^{2+}$, which may result in the ion transmission loss for this system due to space-charge effects. The transmission loss may be reduced by optimizing the potential gradient between the bent flatapole offset and conductance limit, which was kept constant to ensure consistent instrument conditions in all the ESI×n (n = 1−4) modes.

Figure 4a shows mass-selected ion currents obtained for several model analytes used in this study including the perchlorinated *closo*-dodecaborate anion, $B_{12}Cl_{12}^{2-}$ (m/z = 277), an anionic methoxy-oxovanadium cluster, $V_6O_7(OCH_3)_{12}^-$ (m/z = 790), a phosphotungstate anion, $PW_{12}O_{40}^{3-}$ (m/z = 958), and a cationic metal chalcogenide superatomic cluster, $Co_6S_8(PEt_3)_6^+$ (m/z = 1317), in the ESI×1 and ESI×4 modes. On average, we observe a 2.8-fold increase in the mass-selected ion current in the ESI×4 mode as compared to ion currents generated using a single ESI emitter.

Figure 4b shows ion currents obtained for different charge states of a model protein, ubiquitin (M = 8.6 kDa). Ubiquitin ions were generated from an acidic 49.5:49.5:1 methanol/H_2O/CH_3COOH (v/v/v) solution. An LTQ mass spectrum of 5 μM ubiquitin in this solvent shown in Figure S2 displays a charge state distribution centered at 10+, which is consistent with the literature.[62] A 20 μM ubiquitin solution was used to test multiplexing of ubiquitin ion beams in the ESI×4 mode. On average, we observe a 3.1-fold increase in the ion current for different charge states of ubiquitin ranging from 7+ to 13+. Collectively, these results demonstrate the applicability of the multiplexing approach to a broad range of molecular ions.

The results presented so far indicate that orthogonal injection of ion beams from both sides of the ion funnel provides an efficient way for multiplexing of independent ESI sources. The almost proportional increase in the ion current suggests that the individual inlets are effectively decoupled. To test this assertion, we used the ESI×2 mode to examine ion currents generated using different pairs of inlets. As shown in Figure S3, we observe similar ion currents, independent of which of the two inlets are used for ion beam multiplexing. This experiment demonstrates that independent orthogonally injected ion beams introduced at different locations of the ion funnel may be efficiently merged to generate a brighter ion beam.

The stability of the ion current over time is important to both analytical and preparative MS applications. Figure S4 shows the stability of the mass-selected ion current of $B_{12}Cl_{12}^{2-}$ in the ESI×4 mode monitored for ∼1 h. We observe a stable mass-selected ion current of ∼13 nA (or 6.5 nA/charge), which is substantially higher than previously reported ESI ion

https://doi.org/10.1021/acs.analchem.1c02092
Anal. Chem. XXXX, XXX, XXX−XXX

currents achieved in preparative MS applications.[34] This high ion current may be used to achieve a deposition rate of >10 μg of mass-selected ions per day, which substantially improves the efficiency of ion soft landing experiments.

The transmission efficiency of ion funnels strongly depends on the operating pressure and voltages applied to the funnel plates. In particular, the radio frequency (RF) electric field is critical to the radial confinement of the ion cloud. Meanwhile, the direct current (DC) field drives the ions axially through the ion funnel. We examined the effect of the RF and DC fields along with the pressure in the ion funnel on the transmission efficiency of high-intensity multiplexed ion beams of Ru-$(bpy)_3^{2+}$ generated in the ESI×4 mode. In these experiments, the total ion current dominated by $Ru(bpy)_3^{2+}$ ions was measured on the rods of the bent flatapole ion guide to quantify the transmission efficiency of the ion funnel interface. Figure 5a shows the ion current transmitted at different RF

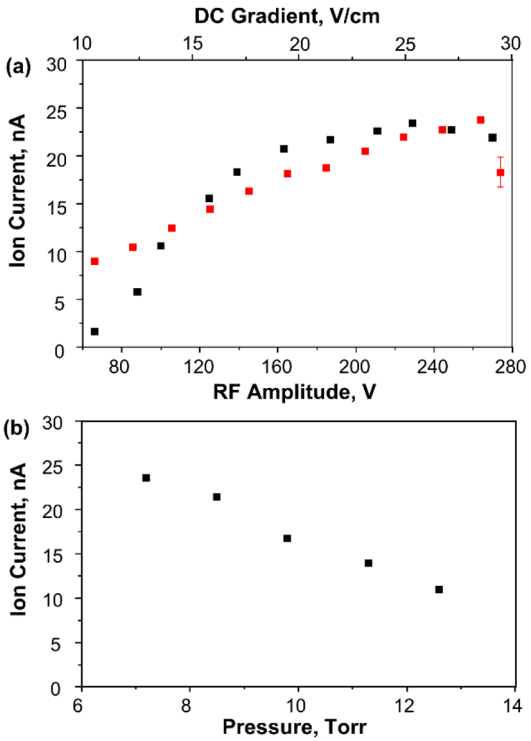

Figure 5. Ion current of $Ru(bpy)_3^{2+}$ as a function of (a) RF amplitude (black), DC gradient (red), and (b) pressure in the HPF.

amplitudes applied to the HPF at a resonance frequency of 740 kHz. The transmission efficiency increases with increase in the RF amplitude and reaches a plateau at 230 $V_{p\text{-}p}$ (peak-to-peak voltage). Further increase in the RF amplitude results in a decrease in transmission. We attribute this decrease in signal to an increase in the low-mass cutoff with an increase in the RF amplitude, which discriminates against lower-m/z ions such as $Ru(bpy)_3^{2+}$. The optimal RF amplitude of 230 $V_{p\text{-}p}$ found for the ESI×4 mode is higher than the typical value of 150 $V_{p\text{-}p}$ used when only two orthogonal inlets are coupled into the ion funnel operated at a similar pressure.[58] This may be attributed to the space-charge-induced expansion of the brighter ion beam produced in the ESI×4 mode, which requires a deeper RF potential well to radially confine the beam. Space-charge effects are determined by the magnitude of the ion current, ion kinetic energy, and volume traversed by the ion beam and may become substantial in the exit region of the HPF, which is confined by a 2.5 mm aperture. In addition, the dynamics of the gas flow in the ESI×4 mode is expected to be distinctly different from that in the ESI×2 mode, in which only two gas flows are introduced from the opposite sides of the ion funnel. This hypothesis will be explored in more detail later in the text.

Figure 5a also shows the transmitted ion current at different DC gradients averaged from three measurements. As described in our previous study,[58] the HPF is composed of a repeller and funnel section. The DC gradient in the repeller section does not have a significant effect on ion transmission. In contrast, the ion current increases with increase in the axial DC gradient in the funnel region. The highest ion current was obtained at a DC gradient of 28 V/cm (320 V DC voltage difference between the first and last electrodes). A further increase in the DC gradient caused a failure of the power supply, which led to a substantially lower and unstable ion current (Figure 5a, ~30 V/cm, DC voltage at 330 V). In the future, we will upgrade the DC power supply to obtain the optimal DC gradient required for multiplexing.

We also studied the effect of pressure in the HPF ion transmission using the RF of 230 $V_{p\text{-}p}$ and a DC of 28 V/cm. The operating pressures in the ion funnels were adjusted by choking the valve on the VARODRY VD 200 mechanical pump evacuating the HPF chamber. We observed a decrease in the ion current with increase in the HPF pressure (Figure 5b), which is in agreement with previous studies, according to which ion diffusion in ion funnels enhanced at higher pressures makes it more difficult to focus the ions using RF and DC fields.[63] The highest ion transmission was observed at the lowest achievable pressure of 7.25 Torr. We expect that ion transmission may be further improved using more powerful vacuum pumps or by increasing the upper limit of the DC power supply to maintain ion transmission at higher HPF pressures.

To obtain further insights into the ion transmission in the ESI×4 mode and rationalize the experimental results, we carried out a series of SIMION ion trajectory simulations combined with gas flow calculations. The simulations were also used to examine the performance of another geometry of the ESI×4 mode, which cannot be currently implemented in our experiments. In particular, we compared the results obtained using the staggered 2 + 2 inlet configuration (two inlets on the two sides of the HPF) implemented in the experiments and aligned 2 + 2 configuration, which will be examined experimentally in future studies.

Figure 6a shows the gas flow velocity in the plane defined by the center of the exit aperture of the HPF and the centers of both cutouts in the repeller region of the HPF. The inlets are located above and below this plane and are equidistant from it. The velocity maps provide insights into gas dynamics inside different regions of the inner space of the HPF. For both the staggered and aligned geometries, the highest gas flow velocity is observed in the HPF repeller region, which is consistent with the previously reported supersonic gas expansion on the vacuum side of capillary inlets. Meanwhile, the flow fields indicate significant differences between the aligned and staggered configurations. Specifically, in the staggered configuration, the different high-speed gas flows exiting the inlets pass each other and move directly to the opposite sides of the HPF with an average gas velocity in the repeller region of >100 m/s. In contrast, in the aligned configuration, the interaction between the high-speed gas flows results in a decrease in the

https://doi.org/10.1021/acs.analchem.1c02092
Anal. Chem. XXXX, XXX, XXX−XXX

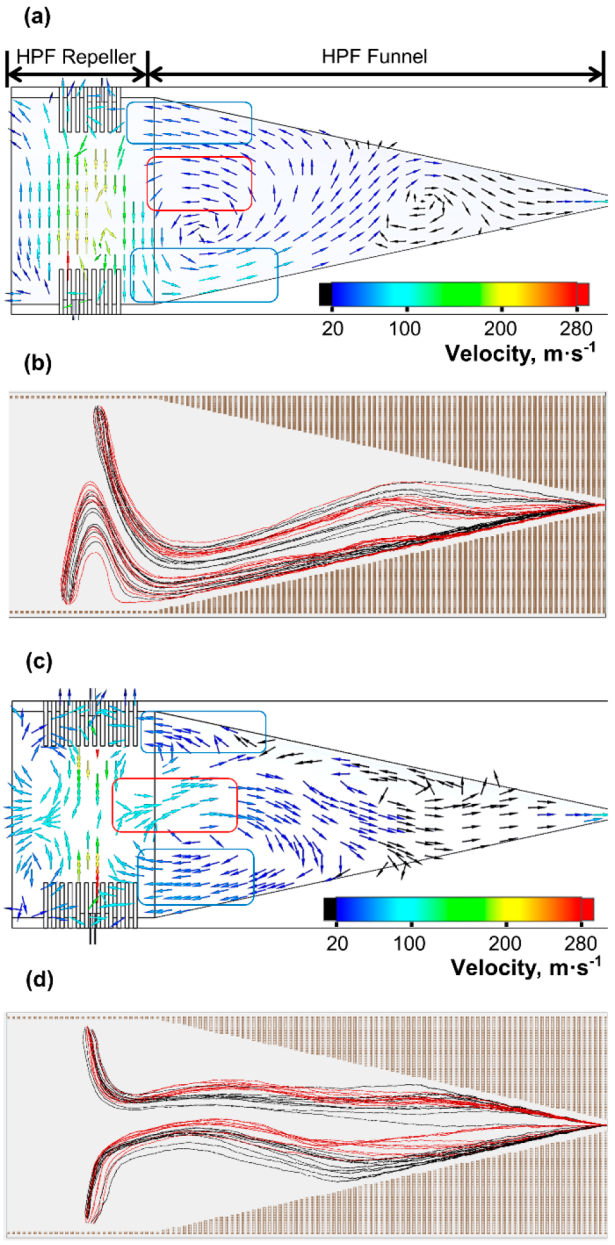

Figure 6. Gas flow velocity field of the HPF along the central plane for the staggered (a) and aligned (c) 2 + 2 inlet configurations. The direction and velocity of the gas flow at a specific location are depicted by the arrows colored according to the velocity scale. The color bar is shown in each panel with velocities below 20 m/s colored in black. The center and off-centered area of the wide opening of the HPF funnel region are marked with red and blue squircles in panels (a) and (c). SIMION simulations of ion trajectories obtained for m/z = 608 in the HPF in the presence of both the gas flow and RF and DC electric fields in the staggered (b) and aligned (d) 2 + 2 inlet configurations.

average gas velocity in the center of the repeller region to ~100 m/s. In both configurations, gas flow velocities decrease to <100 m/s in the funnel region where both gas streams merge and move toward the HPF exit along the instrument axis.

The gas dynamics in the funnel region of the HPF shows substantial differences between the staggered and aligned 2 + 2 configurations. In particular, in the center of the HPF funnel region highlighted by red squircles in Figure 6a,c, gas flow moves upstream in the staggered configuration and downstream in the aligned configuration. In the off-centered locations of the funnel region highlighted with blue squircles, gas flow moves in the opposite directions on the two sides of the HPF when the inlets are in the staggered configuration. In contrast, in the aligned configuration, gas flow moves upstream toward the repeller region on both sides of the HPF. The observed differences in the gas flow dynamics in the staggered and aligned configurations have a pronounced effect on ion trajectories. Figure 6b,d shows ion trajectories in the presence of the same electric field for gas flow fields shown in Figure 6a and 6c for the staggered and aligned 2 + 2 configurations, respectively. In the staggered configuration, ions produced in the upstream inlets shown on the bottom of the diagram initially follow the streams coming out of the inlets. However, they are deflected by the DC field into the incoming jets from the top of the diagram, which deflect the ions toward the electrodes (Figure 6b). Subsequently, the upstream ion trajectories "crawl" along the inner wall of the HPF. This "crawling" is due to the high-speed gas flow in the region between the repeller and funnel section shown in Figure 6a. In this area, gas dynamics dominate over the electric field, turning the ion beam back toward the HPF wall. Meanwhile, ions produced by the downstream inlets shown on the top of the diagram are not blocked by the streams of the other jets and start to make the turn toward the funnel region earlier. In the aligned configuration, in the same region between the repeller and the funnel region of the HPF, gas flow directs the ions to the center of the HPF where they make the turn toward the funnel region (Figure 6c). As a result, we observe close to symmetric ion trajectories from both sides of the HPF that are directed toward the center of the HPF where ions are extracted by the electric field and directed toward the HPF exit. In this configuration, the gas flow keeps the ions away from the electrodes and potentially eliminates ion transmission losses. Regardless of the shape of ion trajectories, SIMION simulations presented in Figure 6b support the experimentally observed additive ion transmission from the four inlets in the ESI×4 mode. Based on the simulation results, we conclude that ion transmission in the aligned 2 + 2 configuration may provide better results than that in the staggered configuration, which was examined experimentally in this study. In the future, we will redesign the HPF chamber to enable multiplexing using the aligned inlet configuration, which will allow us to evaluate the performance of the aligned configuration.

We also carried out simulations to understand the effect of pressure in the HPF on multiplexing. Figure S5 shows gas flow velocity fields and ion trajectories of the 2 + 2 aligned configuration at three different pressures of 11, 7, and 4 Torr. At higher pressures of 11 and 7 Torr (Figure S5a,b), gas flow between the repeller and the funnel region of the HPF is directed downstream along the HPF axis, which is favorable for ion transmission. At a lower pressure of 4 Torr, gas flow in the center of the HPF funnel region moves away from the central axis, which is detrimental to ion transmission. Consequently, the calculated ion trajectories start to diffuse away from the HPF central axis earlier at 4 Torr. This effect is not observed at higher pressures, which rationalizes the improved ion transmission at 7 and 11 Torr. We also observe that at 7 Torr, ion trajectories are kept farthest away from the electrodes. From the pressure-dependent study, we conclude that 7 Torr is the optimal HPF pressure for multiplexing of ESI sources using the 2 + 2 aligned configuration. We note that although the

https://doi.org/10.1021/acs.analchem.1c02092
Anal. Chem. XXXX, XXX, XXX−XXX

simulations were performed with a temperature of the inlet tubes of 305 K, we anticipate qualitatively similar results at higher temperatures of ∼450 K used experimentally. Reiss et al. have demonstrated that the maximum gas flow velocity through a heated inlet increases by <10 m/s with a temperature increase from 350 to 550 K.[30] Interestingly, the maximum gas velocity is observed ∼0.2 mm off the inlet axis at 550 K. The relatively small increase in gas velocity and small offset off the inlet tube axis will not affect to a significant extent the results of the gas flow and ion trajectory simulations reported herein.

CONCLUSIONS

In this study, we demonstrate that orthogonal injection of ions into an electrodynamic ion funnel is a promising approach for the multiplexing of independent ESI sources. In particular, we used a total of four orthogonal inlets that were split into two pairs and implemented on the opposite sides of the ion funnel. For the different types of analytes used in our proof-of-concept experiments, we observed an almost proportional increase in both the ion current and SNR with increase in the number of orthogonal inlets used for ion beam injection. Using the optimized values of the instrument parameters including the RF amplitude, axial DC gradient, and pressure in the HPF, we have achieved a maximum mass-selected ion current of up to 7 nanoamperes per charge, which corresponds to the deposition of >10 μg of mass-selected ions per day, substantially higher than the typical deposition rate of ∼1 μg with a single ESI source. The bright ion source developed in this study provides a direct path for materials synthesis and device fabrication using beams of mass-selected ions. Furthermore, analytical MS applications would benefit from this mode of multiplexing, which increases the SNR in proportion to the number of inlets. The experimental results were rationalized using the combined gas flow and ion trajectory simulations. The simulations were further employed to examine the aligned inlet configuration, which could not be implemented experimentally. Based on the simulation results, we conclude that it is possible to further optimize the geometry of the multiplexing configuration. We envision that multiplexing of more than four ESI sources is possible using more powerful mechanical pumps to maintain the pressure in the HPF at its optimal value. In addition to preparative MS applications, multiplexed ESI sources may be implemented on commercial analytical mass spectrometers, which will improve their performance in analytical applications including multiomics studies, single-cell analysis, and biomolecular imaging.

ASSOCIATED CONTENT

Supporting Information

The Supporting Information is available free of charge at https://pubs.acs.org/doi/10.1021/acs.analchem.1c02092.

Description of RWMA; Figure S1: Schematic diagram of the high-transmission ESI interface; Figure S2: ESI-MS spectrum of ubiquitin; Figure S3. Mass-selected ion current of $B_{12}Cl_{12}^{2-}$ in the ESI×2 mode; Figure S4. Long-term stability of ion current of $B_{12}Cl_{12}^{2-}$; Figure S5. Gas flow velocity fields and ion trajectories at different pressures (PDF)

AUTHOR INFORMATION

Corresponding Author

Julia Laskin − *Department of Chemistry, Purdue University, West Lafayette, Indiana 47907, United States;* orcid.org/0000-0002-4533-9644; Phone: 765-494-5464; Email: jlaskin@purdue.edu

Authors

Pei Su − *Department of Chemistry, Purdue University, West Lafayette, Indiana 47907, United States;* orcid.org/0000-0001-6148-0181

Xi Chen − *Department of Mechanical and Energy Engineering, Indiana University−Purdue University Indianapolis, Indianapolis, Indiana 46202, United States*

Andrew J. Smith − *Department of Chemistry, Purdue University, West Lafayette, Indiana 47907, United States*

Michael F. Espenship − *Department of Chemistry, Purdue University, West Lafayette, Indiana 47907, United States;* orcid.org/0000-0003-1174-3347

Hugo Y. Samayoa Oviedo − *Department of Chemistry, Purdue University, West Lafayette, Indiana 47907, United States;* orcid.org/0000-0001-9024-7071

Solita M. Wilson − *Department of Chemistry, Purdue University, West Lafayette, Indiana 47907, United States*

Habib Gholipour-Ranjbar − *Department of Chemistry, Purdue University, West Lafayette, Indiana 47907, United States*

Carlos Larriba-Andaluz − *Department of Mechanical and Energy Engineering, Indiana University−Purdue University Indianapolis, Indianapolis, Indiana 46202, United States;* orcid.org/0000-0003-0864-7733

Complete contact information is available at: https://pubs.acs.org/10.1021/acs.analchem.1c02092

Author Contributions

[§]P.S. and X.C. contributed equally to this work.

Notes

The authors declare no competing financial interest.

[‖]Undergraduate researcher. (A.J.S.)

ACKNOWLEDGMENTS

The authors thank the Jonathan Amy Facility for Chemical Instrumentation staff for technical support, Dr. Jonas Warneke (Universität Leipzig, Germany) for valuable suggestions, and Prof. Carsten Jenne (University of Wuppertal, Germany) for providing $B_{12}Cl_{12}^{2-}$ salts for our experiments. This work is also supported by the National Science Foundation Division of Chemistry under Grant No. 1904879 (Program officer Dr. Kelsey Cook).

REFERENCES

(1) Fenn, J. B.; Mann, M.; Meng, C. K.; Wong, S. F.; Whitehouse, C. M. *Science* **1989**, *246*, 64.

(2) Fenn, J. B.; Mann, M.; Meng, C. K.; Wong, S. F.; Whitehouse, C. M. *Mass Spectrom. Rev.* **1990**, *9*, 37−70.

(3) Kebarle, P.; Tang, L. *Anal. Chem.* **1993**, *65*, 972A−986A.

(4) Cole, R. B. *J. Mass Spectrom.* **2000**, *35*, 763−772.

(5) Chowdhury, S. K.; Katta, V.; Chait, B. T. *Rapid Commun. Mass Spectrom.* **1990**, *4*, 81−87.

(6) Loo, J. A. *Mass Spectrom. Rev.* **1997**, *16*, 1−23.

(7) Niessen, W. M. *Liquid chromatography-mass spectrometry*, 3rd ed.; CRC Press, 2006.

(8) Smith, R. D.; Barinaga, C. J.; Udseth, H. R. *Anal. Chem.* **1988**, *60*, 1948−1952.
(9) Wenk, M. R.; Lucast, L.; Di Paolo, G.; Romanelli, A. J.; Suchy, S. F.; Nussbaum, R. L.; Cline, G. W.; Shulman, G. I.; McMurray, W.; De Camilli, P. *Nat. Biotechnol.* **2003**, *21*, 813−817.
(10) Di Marco, V. B.; Bombi, G. G. *Mass Spectrom. Rev.* **2006**, *25*, 347−379.
(11) Rauschenbach, S.; Stadler, F. L.; Lunedei, E.; Malinowski, N.; Koltsov, S.; Costantini, G.; Kern, K. *Small* **2006**, *2*, 540−547.
(12) Johnson, G. E.; Gunaratne, D.; Laskin, J. *Mass Spectrom. Rev.* **2016**, *35*, 439−479.
(13) Verbeck, G.; Hoffmann, W.; Walton, B. *Analyst* **2012**, *137*, 4393−4407.
(14) Cyriac, J.; Pradeep, T.; Kang, H.; Souda, R.; Cooks, R. *Chem. Rev.* **2012**, *112*, 5356−5411.
(15) Sharon, M.; Robinson, C. V. *Annu. Rev. Biochem.* **2007**, *76*, 167−193.
(16) Takats, Z.; Wiseman, J. M.; Cooks, R. G. *J. Mass Spectrom.* **2005**, *40*, 1261−1275.
(17) Kujawinski, E. B.; Freitas, M. A.; Zang, X.; Hatcher, P. G.; Green-Church, K. B.; Jones, R. B. *Org. Geochem.* **2002**, *33*, 171−180.
(18) Papac, D. I.; Shahrokh, Z. *Pharm. Res.* **2001**, *18*, 131−145.
(19) Zhang, J.; Rector, J.; Lin, J. Q.; Young, J. H.; Sans, M.; Katta, N.; Giese, N.; Yu, W.; Nagi, C.; Suliburk, J. *Sci. Transl. Med.* **2017**, *9*, eaan3968.
(20) Santagata, S.; Eberlin, L. S.; Norton, I.; Calligaris, D.; Feldman, D. R.; Ide, J. L.; Liu, X.; Wiley, J. S.; Vestal, M. L.; Ramkissoon, S. H.; et al. *Proc. Natl. Acad. Sci. U. S. A.* **2014**, *111*, 11121−11126.
(21) Laskin, J.; Johnson, G. E.; Warneke, J.; Prabhakaran, V. *Angew. Chem., Int. Ed.* **2018**, *57*, 16270−16284.
(22) Rauschenbach, S.; Rinke, G.; Malinowski, N.; Weitz, R. T.; Dinnebier, R.; Thontasen, N.; Deng, Z.; Lutz, T.; de Almeida Rollo, P. M.; Costantini, G.; et al. *Adv. Mater.* **2012**, *24*, 2761−2767.
(23) Prabhakaran, V.; Mehdi, B. L.; Ditto, J. J.; Engelhard, M. H.; Wang, B.; Gunaratne, K. D. D.; Johnson, D. C.; Browning, N. D.; Johnson, G. E.; Laskin, J. *Nat. Commun.* **2016**, *7*, 11399.
(24) Su, P.; Prabhakaran, V.; Johnson, G. E.; Laskin, J. *Anal. Chem.* **2018**, *90*, 10935−10942.
(25) Roy, C.; Sebok, B.; Scott, S. B.; Fiordaliso, E. M.; Sørensen, J. E.; Bodin, A.; Trimarco, D. B.; Damsgaard, C. D.; Vesborg, P. C. K.; Hansen, O.; Stephens, I. E. L.; Kibsgaard, J.; Chorkendorff, I. *Nat. Catal.* **2018**, *1*, 820−829.
(26) Palmer, R. E.; Cai, R.; Vernieres, J. *Acc. Chem. Res.* **2018**, *51*, 2296−2304.
(27) Pepi, F.; Ricci, A.; Tata, A.; Favero, G.; Frasconi, M.; Delle Noci, S.; Mazzei, F. *Chem. Commun.* **2007**, 3494−3496.
(28) Cox, J. T.; Marginean, I.; Smith, R. D.; Tang, K. *J. Am. Soc. Mass Spectrom.* **2015**, *26*, 55−62.
(29) Page, J. S.; Marginean, I.; Baker, E. S.; Kelly, R. T.; Tang, K.; Smith, R. D. *J. Am. Soc. Mass Spectrom.* **2009**, *20*, 2265−2272.
(30) Bernier, L.; Taesch, M.; Rauschenbach, S.; Reiss, J. *Int. J. Mass Spectrom.* **2020**, *447*, 116239.
(31) Kim, T.; Udseth, H. R.; Smith, R. D. *Anal. Chem.* **2000**, *72*, 5014−5019.
(32) Wu, S.; Zhang, K.; Kaiser, N. K.; Bruce, J. E.; Prior, D. C.; Anderson, G. A. *J. Am. Soc. Mass Spectrom.* **2006**, *17*, 772−779.
(33) Pauly, M.; Sroka, M.; Reiss, J.; Rinke, G.; Albarghash, A.; Vogelgesang, R.; Hahne, H.; Kuster, B.; Sesterhenn, J.; Kern, K.; Rauschenbach, S. *Analyst* **2014**, *139*, 1856−1867.
(34) Gunaratne, K. D. D.; Prabhakaran, V.; Ibrahim, Y. M.; Norheim, R. V.; Johnson, G. E.; Laskin, J. *Analyst* **2015**, *140*, 2957−2963.
(35) Page, J. S.; Tang, K.; Kelly, R. T.; Smith, R. D. *Anal. Chem.* **2008**, *80*, 1800−1805.
(36) Meier, L.; Berchtold, C.; Schmid, S.; Zenobi, R. *Anal. Chem.* **2012**, *84*, 2076−2080.
(37) Ahmed, E.; Xiao, D.; Kabir, K. M. M.; Fletcher, J.; Donald, W. A. *Anal. Chem.* **2020**, *92*, 15811−15817.
(38) Smith, J. N.; Flagan, R. C.; Beauchamp, J. L. *J. Phys. Chem. A* **2002**, *106*, 9957−9967.
(39) Konermann, L.; Ahadi, E.; Rodriguez, A. D.; Vahidi, S. *Anal. Chem.* **2013**, *85*, 2−9.
(40) De La Mora, J. F.; Loscertales, I. G. *J. Fluid Mech.* **1994**, *260*, 155−184.
(41) Su, S.; Gibson, G. T. T.; Mugo, S. M.; Marecak, D. M.; Oleschuk, R. D. *Anal. Chem.* **2009**, *81*, 7281−7287.
(42) Kim, W.; Guo, M.; Yang, P.; Wang, D. *Anal. Chem.* **2007**, *79*, 3703−3707.
(43) Fu, Y.; Gibson, G. T. T.; Proulx, A.; Croteau, A.; Schneider, B. B.; Covey, T. R.; Oleschuk, R. D. *Anal. Chem.* **2015**, *87*, 747−753.
(44) Kelly, R. T.; Page, J. S.; Zhao, R.; Qian, W.-J.; Mottaz, H. M.; Tang, K.; Smith, R. D. *Anal. Chem.* **2008**, *80*, 143−149.
(45) Johnson, G. E.; Prabhakaran, V.; Browning, N. D.; Mehdi, B. L.; Laskin, J.; Kottke, P. A.; Fedorov, A. G. *Batteries & Supercaps* **2018**, *1*, 97−101.
(46) Mao, P.; Gomez-Sjoberg, R.; Wang, D. *Anal. Chem.* **2013**, *85*, 816−819.
(47) Shen, Y.; Tolić, N.; Zhao, R.; Paša-Tolić, L.; Li, L.; Berger, S. J.; Harkewicz, R.; Anderson, G. A.; Belov, M. E.; Smith, R. D. *Anal. Chem.* **2001**, *73*, 3011−3021.
(48) Lenguito, G.; Fernandez de la Mora, J.; Gomez, A. *J. Micromech. Microeng.* **2014**, *24*, No. 055003.
(49) Sochorakis, N.; Grifoll, J.; Rosell-Llompart, J. *Chem. Eng. Sci.* **2019**, *195*, 281−298.
(50) Kelly, R. T.; Page, J. S.; Marginean, I.; Tang, K.; Smith, R. D. *Anal. Chem.* **2008**, *80*, 5660−5665.
(51) Iyer, K.; Marsh, B. M.; Capek, G. O.; Schrader, R. L.; Tichy, S.; Cooks, R. G. *J. Am. Soc. Mass Spectrom.* **2019**, *30*, 2584−2593.
(52) Baird, Z.; Wei, P.; Cooks, R. G. *Analyst* **2015**, *140*, 696−700.
(53) Shaffer, S. A.; Prior, D. C.; Anderson, G. A.; Udseth, H. R.; Smith, R. D. *Anal. Chem.* **1998**, *70*, 4111−4119.
(54) Kelly, R. T.; Tolmachev, A. V.; Page, J. S.; Tang, K.; Smith, R. D. *Mass Spectrom. Rev.* **2010**, *29*, 294−312.
(55) Chen, T.-C.; Fillmore, T. L.; Prost, S. A.; Moore, R. J.; Ibrahim, Y. M.; Smith, R. D. *Anal. Chem.* **2015**, *87*, 7326−7331.
(56) Gholipour-Ranjbar, H.; Fang, H.; Guan, J.; Peters, D. A.; Seifert, A.; Jena, P.; Laskin, J. *Small* **2021**, *17*, 2002927.
(57) Daniel, C.; Hartl, H. *J. Am. Chem. Soc.* **2005**, *127*, 13978−13987.
(58) Su, P.; Hu, H.; Warneke, J.; Belov, M. E.; Anderson, G. A.; Laskin, J. *Anal. Chem.* **2019**, *91*, 5904−5912.
(59) Su, P.; Hu, H.; Unsihuay, D.; Zhang, D.; Dainese, T.; Diaz, R. E.; Lee, J.; Gunaratne, D. K.; Wang, H.; Maran, F.; Mei, J.; Laskin, J. *Angew. Chem., Int. Ed.* **2020**, *59*, 7711−7716.
(60) Su, P.; Espenship, M. F.; Laskin, J. *J. Am. Soc. Mass Spectrom.* **2020**, *31*, 1875−1884.
(61) McAlister, G. C.; Phanstiel, D.; Good, D. M.; Berggren, W. T.; Coon, J. J. *Anal. Chem.* **2007**, *79*, 3525−3534.
(62) Konermann, L.; Douglas, D. *J. Am. Soc. Mass Spectrom.* **1998**, *9*, 1248−1254.
(63) Ibrahim, Y.; Tang, K.; Tolmachev, A. V.; Shvartsburg, A. A.; Smith, R. D. *J. Am. Soc. Mass Spectrom.* **2006**, *17*, 1299−1305.

https://doi.org/10.1021/acs.analchem.1c02092
Anal. Chem. XXXX, XXX, XXX−XXX